Journal of Energy Storage 52 (2022) 104789

Contents lists available at ScienceDirect

Journal of Energy Storage

journal homepage: www.elsevier.com/locate/est

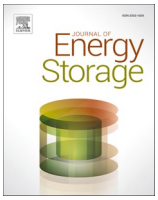

Research Papers

Safety boundary of power battery based on quantitative lithium deposition

Hang Li [a], Weijie Ji [a], Peng Zhang [b,*,1], Jinbao Zhao [a,*,1]

[a] State Key Lab of Physical Chemistry of Solid Surfaces, Collaborative Innovation Centre of Chemistry for Energy Materials, State-Province Joint Engineering Laboratory of Power Source Technology for New Energy Vehicle, Engineering Research Center of Electrochemical Technology, Ministry of Education, College of Chemistry and Chemical Engineering, Xiamen University, Xiamen 361005, PR China

[b] College of Energy & School of Energy Research, Xiamen University, Xiamen 361102, Fujian, China

ARTICLE INFO

Keywords:
Thermal runaway
Safety prediction
Fast-charging
Quantitative lithium deposition

ABSTRACT

There are not perfect ways to solve the lithium metal deposition of the lithium-ion battery during the fast-charging process currently. Moreover, the safety problems caused by lithium deposition are also unfixed. The safety boundary will be a practical guide for battery usage. In this research, batteries designed with different capacities are charged to achieve different lithium deposition and establish prediction data for battery safety boundaries based on the safety performance of the batteries. The quantitative method of lithium deposition combined with the safe behavior of the battery provides an important reference method for the design of fast charging of the battery. What's more excited is that our approach is expanded to provide experience for the manufacturers in battery safety design that can meet the different fast charging rate requirements. The safety boundaries can achieve the best battery safety performance while saving the materials consumed in manufacture from the root.

1. Introduction

As an energy carrier, lithium-ion batteries are being widely used to achieve the goal of carbon neutrality [1,2]. Despite lithium-ion batteries have many advantages, there are still shortcomings that limit their further widespread use: safety anxiety, charge anxiety and mileage anxiety [3–6].

These factors are inherent shortcomings of batteries and are seriously related to battery materials. In addition, the battery cannot reach a large capacity and high safety in short time. Commercial use of high-capacity materials with fast charge rate cannot be solved overnight. Fast charge, especially the ultrafast charge, has been the dramatically need for power battery [7–10]. However, lithium deposition inevitably occurs in lithium-ion batteries during the fast charge, which will seriously affect the cycle life and safety of the battery [7,11–16]. The lithium ion in the battery can't insert into the material yet through electrochemical reactions, or react with the electrode material, therefore the lithium metal will deposit on the surface of the material [17–20]. There are some ways to control lithium deposition in the lithium ion battery, such as optimizing the design of the battery (such as the thickness, length of the electrode, and so on), promoting the performance of the material (negative electrode material, electrolyte, separator, and so on), optimizing the charging profiles (constant current-constant voltage, pulse charging, feedback charging, and so on) [21–27]. Nevertheless, the method above can't address the dangerous of lithium deposition from the origin and predict the safety of the battery.

Therefore, we sincerely believe that the solution to lithium deposition during the fast charge could be based on the design of the battery itself. Moreover, the safety prediction will encourage the extensive apply of lithium ion battery. In spite of various lithium deposition effects in the lithium-ion battery, all the factors can be generally summarized as two sections: kinetics and thermodynamics [28–34]. While, these factors are not entirely independent. They are highly consistent with the battery itself as a complete and complex system. Hence, to solve the problem of lithium deposition, it should be a more promising way to solve the problem from an engineering perspective [35–38]. Quantifying lithium deposition in batteries and establishing an equivalence relationship with battery safety based on the amount of lithium deposition is urgently needed to be studied.

Here, the safety boundary of lithium-ion batteries during the fast charge was discussed in our research. Based on the constant compacted density of negative electrode, we design the $LiNi_{0.8}Co_{0.1}Mn_{0.1}O_2$ /

* Corresponding authors.
E-mail address: jbzhao@xmu.edu.cn (J. Zhao).
[1] The two authors have the same contribution to this study.

https://doi.org/10.1016/j.est.2022.104789
Received 21 February 2022; Received in revised form 20 April 2022; Accepted 1 May 2022
Available online 7 May 2022

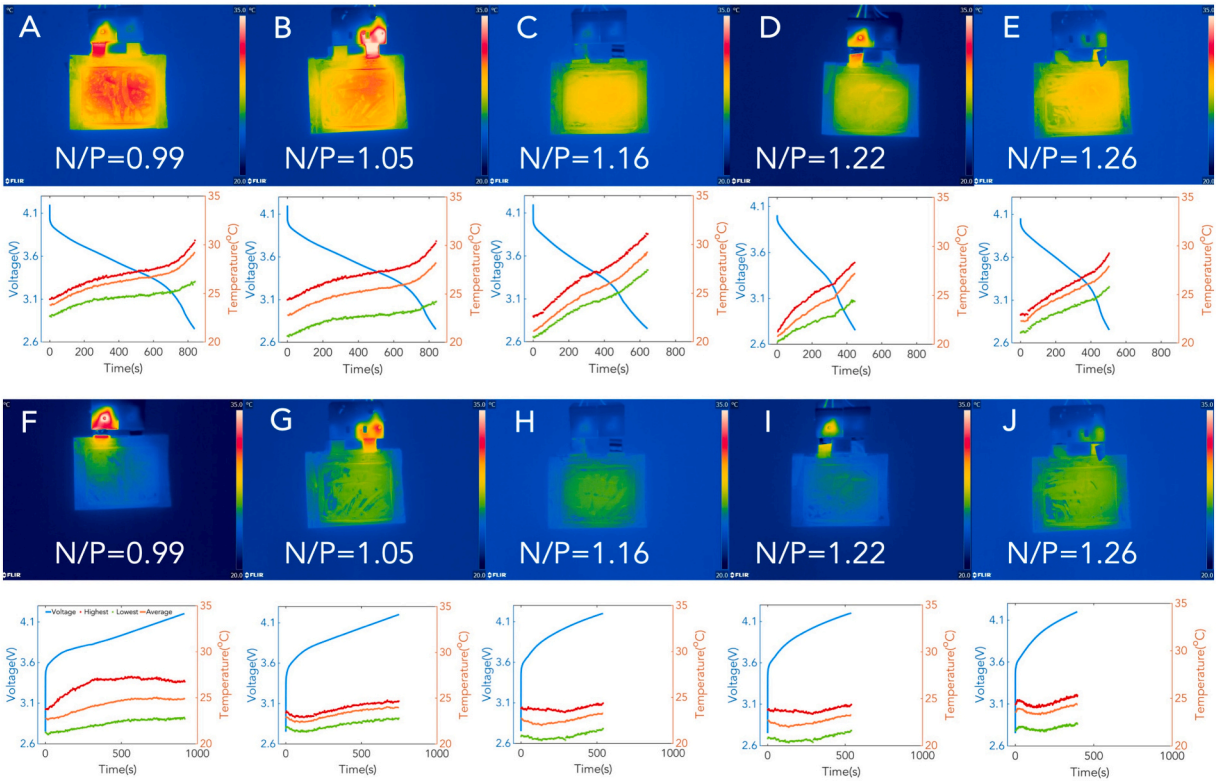

Fig. 1. IR shows the temperature of the battery.
The (A), (B), (C), (D), (E) correspond to the time of the battery at the end of discharging, and the line graph below shows the temperature (the highest, lowest, average temperature in the surface of the battery) and voltage changes during battery discharge. Similarly, the (F), (G), (H), (I), (J) correspond to the time of the battery at the end of the charge. The temperature change during the discharge process is more obvious than that in the charge process.

graphite batteries with different areal capacity ratios of negative to positive electrodes (N/P) by controlling the positive electrode capacity to be constant. The safety criteria of the batteries with different amount of lithium deposition were investigated. The safety boundary of the battery was determined through simulation and quantitative data. The prediction result will help the design and usage of fast-charge lithium-ion battery to prevent danger occurring.

2. Experimental

The N/P ratio was used to control the different amounts of lithium deposition. The N/P was defined based on the electrode at same compacted density in this research. The battery was tested after 5 cycles at the rate of 3 C (5.4 A) in room temperature. We chose the 3 C in the measurement was to get the fast charge target of fully charged in 20 min. Through qualifying the amounts of lithium deposition, the battery safety boundary index map was predicted by the linear regression.

2.1. Battery manufacture

The positive material used the $LiNi_{0.8}Co_{0.1}Mn_{0.1}O_2$, the negative material used the natural graphite. The design capacity of the pouch lithium-ion battery was 1.8 Ah, which the specific capacity of the positive and negative was 220 $mAh{\cdot}g^{-1}$ and 330 $mAh{\cdot}g^{-1}$ respectively. Other parameters of the battery were listed in the support information.

2.2. Electrochemical test

The constant current (CC) stage current of the formation process was set to 0.1 C (0.180 A), and the cut-off current in the constant voltage (CV) stage is 0.01 C (0.018 A). Besides, the discharge current was set to constant current 0.1 C (0.180 A). After 5 cycles at the rate of 3 C, the battery was used for the post-mortem and ARC test. All batteries were cycled between 2.75 and 4.2 V. For the galvanostatic intermittent titration technique (GITT) measurements, the pulse current density was 0.1 C and the pulse time was 10 min, followed by a relaxation time of 2 h.

2.3. Thermal test

The battery was fully charged (4.2 V) before the adiabatic accelerated calorimetry (ARC) test. The starting temperature was set to 40 °C and the heating step was 5 °C. The detected self-heating rate was 0.02 °C min^{-1} and the waiting time was 30 min. The electrode material was scraped by a scalpel for the DSC test. The test process is heated from 35 °C to 400 °C at a rate of 10 °C min^{-1}.

2.4. Simulation

The simulation platform used the COMSOL Multiphysics. The model used in the lithium-ion battery was built by Neman et al., which was a one-dimensional model. The lithium deposition was added as the side reaction. The parameters used in the model were listed in the support information. The linear regression was calculated by the Matlab.

3. Result & discussion

3.1. Lithium deposition characterize

The thermal perspective can be the path for lithium deposition diagnostics due to the thermal change during the lithium deposition process [36–39]. The Infrared camera (IR) would be used as the simplest way to monitor the heat generation of the batteries. The lithium deposition behavior will affect the heat generation and heat generation

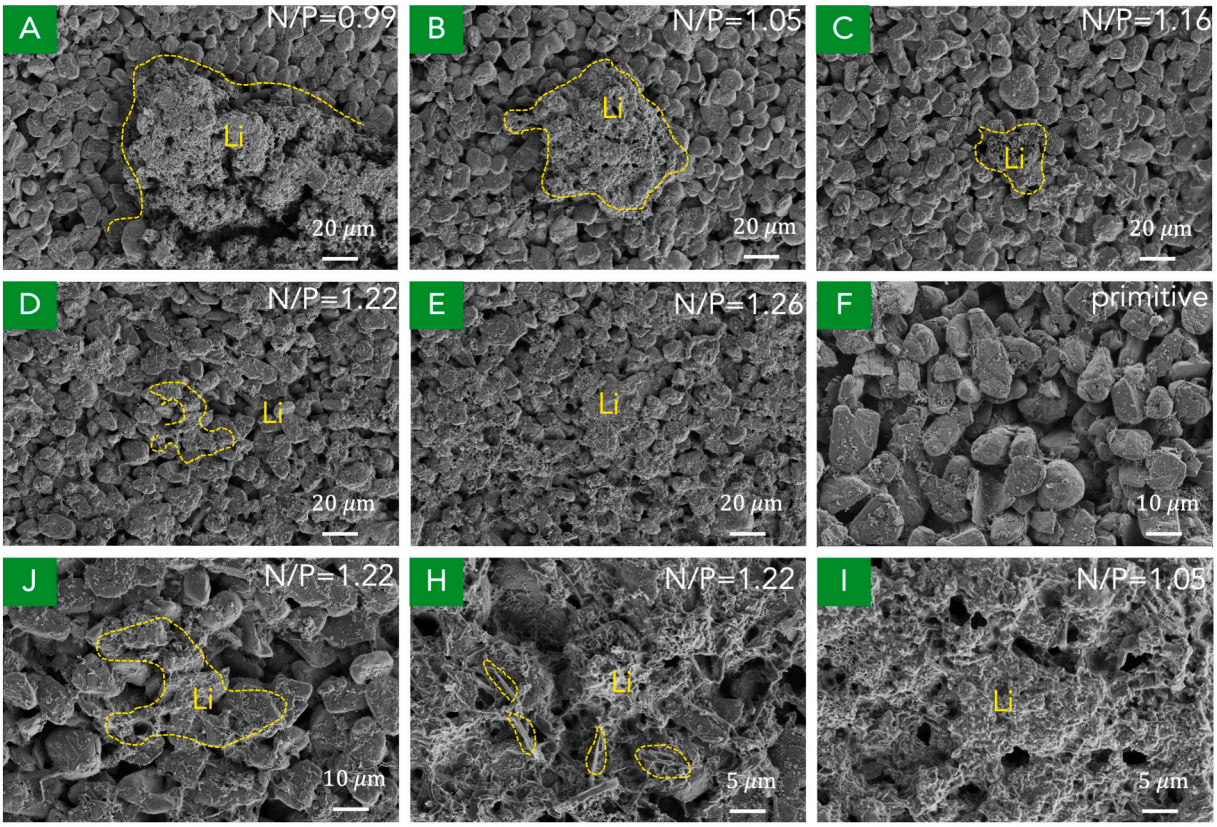

Fig. 2. Images showing the graphite SEM of different N/P battery.
Characterization of the morphology evolution of graphite electrode with different lithium deposition. The different pictures correspond to different N/P and scale. The size of the deposited lithium first decreases and then increases with the N/P value. The morphology also changed from moss-like to dendrites that are highly related to the electrochemical properties of the battery.

power of the battery. Therefore, the clues of lithium deposition expected to be explored through IR. The batteries were charged and discharged in the same environment (room temperature was constant, and the charge/discharge current rate was 3 C (5.4 A). The test of the charging and discharging process was independent that the batteries were standing in the environment for two hours to reach the room temperature before the IR test. The IR results show that the temperature will significantly change during the discharging process, while the temperature change can hardly be observed during the charging process (Fig. 1). The temperature increased about 5 °C during the discharge process (Fig. 1(A)–(E)), especially for the battery with the N/P of 0.99 whose the temperature increased by 7.6 °C (Fig. 1(A)). However, as shown in Fig. 1(F)–(J), the temperature slightly increased about 1 °C during the charging process. The IR pictures straightly show the temperature state of the battery when the charge/discharge ends. Moreover, the effect of current on heat generation was evident in that the highest temperature of the battery was near the battery tabs.

Comparing to the discharge process, the relatively low temperature change makes it more difficult to characterize lithium deposition during charging. The temperature change during the battery charging process was not a fast channel to judge the lithium deposition characteristics. Due to the influence of the cell size, the heat dissipation of the battery will significantly change. There is heat generation due to lithium deposition in the cell, but this kind of heat too little to observed when using the battery. On the contrary, the distinct temperature change can be observed during the discharge process (the lithium dissolve process during the discharge process, as the reverse process of lithium deposition). This change may be related to the extra heat generated by the solvation reaction during the re-dissolution process of the lithium deposition. From the macroscopic view, it can be considered that the detection of lithium deposition in the battery has an inevitable hysteresis.

The batteries were disassembled to observe the lithium deposition intuitively. The fully charged battery was disassembled in the glove box (the battery has been charged and discharged for 5 cycles in the room at the charge/discharge current rate of 3 C, and the cut-off voltage was 2.75–4.2 V). The scanning electron microscopy (SEM) was used to record the morphology of the electrode. There was a large moss-like of lithium deposition on the surface of the graphite electrode when the N/P value was 0.99 (Fig. 2(A)). With the increase of the N/P, the lithium deposition becomes smaller and finally becomes the dendritic morphology. Moreover, the dendritic deposition becomes more uniform with the increase of the N/P. Especially the battery with N/P of 1.26 (Fig. 2(E)), the uniform deposition likely to form on the material surface.

The photos of the battery's electrodes show the change in the amount of lithium deposition. As shown in Fig. S1(A)–(E), the local deposition of the lithium deposition can be observed. Moreover, it can be clearly seen that a large amount of lithium metal was deposited on the side of the separator close to the negative electrode (Fig. S1(F)–(J)), and with the increase of the N/P value, the amount of deposition decreased firstly and then increased. Surprisingly, the deposited lithium was almost invisible on the separator when the battery's N/P value was 1.16 (Fig. S1(H)). Besides, for battery safety regulation strategies, it is more important to change the separator near the side of the negative electrode.

We attempt to study the inducing factors of Li metal deposition morphology and the resulting safety issues. Lithium deposition in the battery is undoubtedly a product of the electrochemical side reaction. From the electrochemical point of view, different products are caused by changing the properties of the negative electrode. Thus, the electrochemistry of the negative electrode should the starting point for

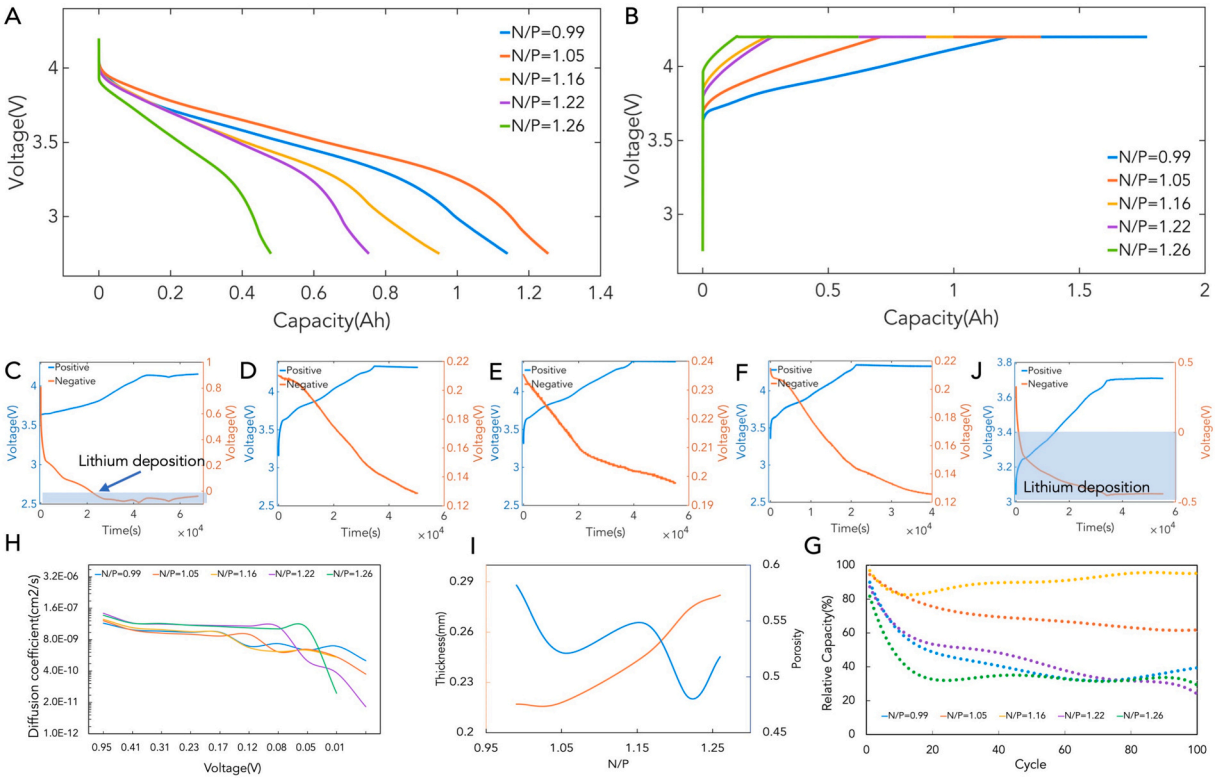

Fig. 3. Electrochemical performance of the battery.
The design capacity of the battery was 1.8 Ah. ((A), (B), (G)) The electrochemical performance which was measured at the rate of 3 C. ((C), (D), (E), (F), (J)) The electrode potential corresponded to the N/P value of 0.99, 1.05, 1.16, 1.22, 1.26, and measured at the rate of 0.1 C. (H) The diffusion coefficient of graphite which was characterized by GITT. The diffusion coefficient of different negative electrode was measured by button batteries with lithium metal as the counter electrode. Lithium deposition that occurs in lithium-ion batteries has a detrimental effect on the electrochemistry of the battery. In addition, the lithium deposition is affected by the properties of the battery electrode.

analysis. As the N/P value increases, the diffusion kinetics of Li-ion batteries should be affected. Therefore, we speculate that the negative electrode does not provide enough space for Li ion insertion at low N/P values, which leads to the aggregation and precipitation of the electrode at the sites preferentially filled with Li, which is the reason for the moss-like deposition. However, with the increase of N/P value, the diffusion kinetics of lithium ions in the negative electrode weakens, resulting in the formation of distributed dendritic deposits on the surface of electrode. Therefore, more electrochemical properties of the negative electrode need to be investigated.

3.2. *Electrochemical performance and simulation*

The change of the N/P value affects the lithium deposition, and this change was also directly reflected in the charge and discharge capacity of the battery. As the N/P value increases, the discharge capacity does not follow a constant trend (with the N/P increased, the capacity tends to constantly increased or decreased). For example, the discharge capacity of the battery with the N/P ratio of 1.16 was 1.25 Ah (Fig. 3(A)), which was higher than other batteries with a higher or lower N/P ratio. However, the change of charging capacity decreases as the value of N/P increases (Fig. 3(B)). Therefore, a proper N/P value was conducive to release of all the designed capacity of the battery and will avoid lithium deposition. It was not worth that blindly increasing the N/P value to improve the safety of the battery in the fast-charging state loses a lot of usable capacity. Meanwhile, the capacity degradation of the battery also shows the same trend of change as the discharge capacity of the battery (Fig. 3(G)). The battery with the NP value of 1.16 maintains a higher capacity retention rate after 100 cycles, but other batteries all show a sharply fade rate, especially the capacity of the battery with the N/P value is 0.99 sharply decreased to the 22% initial discharge capacity after 100 cycles. The electrode potential change has been monitored at the same time by placing a lithium metal reference electrode in the pouch cell. As the charge progresses, the electrode potential will be lower than 0 V when the negative electrode with the lowest N/P (Fig. 3 (C)). Even if it was charged at a lower rate (0.1 C), there've still presented lithium deposition. In the case of the highest N/P (1.26), the potential of the graphite negative electrode will quickly be lower than 0 V (Fig. 3(J)). Herein, there is no doubt that the lithium deposition would take on the electrode. Moreover, the electrode potential is always lower than 0 V during the charging process indicated that lithium deposition will occur on the entire electrode. The uniform deposition can be attached to the fact that the entire electrode was lower than 0 V so that the lithium deposition occurred without distinguishing positions.

The change of potential has a more extraordinary relation with the physical characteristics of the graphite electrode. The resistivity and porosity of the graphite electrode were measured by using dry electrodes. As the increase of the electrode thickness, the resistivity was held to a constant value (0.069 m**Ω**/mm) (Fig. S2), especially when the electrodes with low N/P. However, the porosity of the electrode considerably decreased over the thickness (Fig. 3(I)). While the change in the resistivity was slight, the overpotential of the electrode surface still increases with the thickness of the electrode if only the ohmic polarization was taken into account. However, the reduction of porosity increases the concentration polarization in the electrode, which further extremely increasing the overpotential on the electrode surface. It exacerbates the generation of lithium deposit in the battery.

Additional, appropriately increasing the N/P value can ensure that the negative electrode runs at a low SOC, thereby improving the fast-charging performance of the battery. However, the limitation of

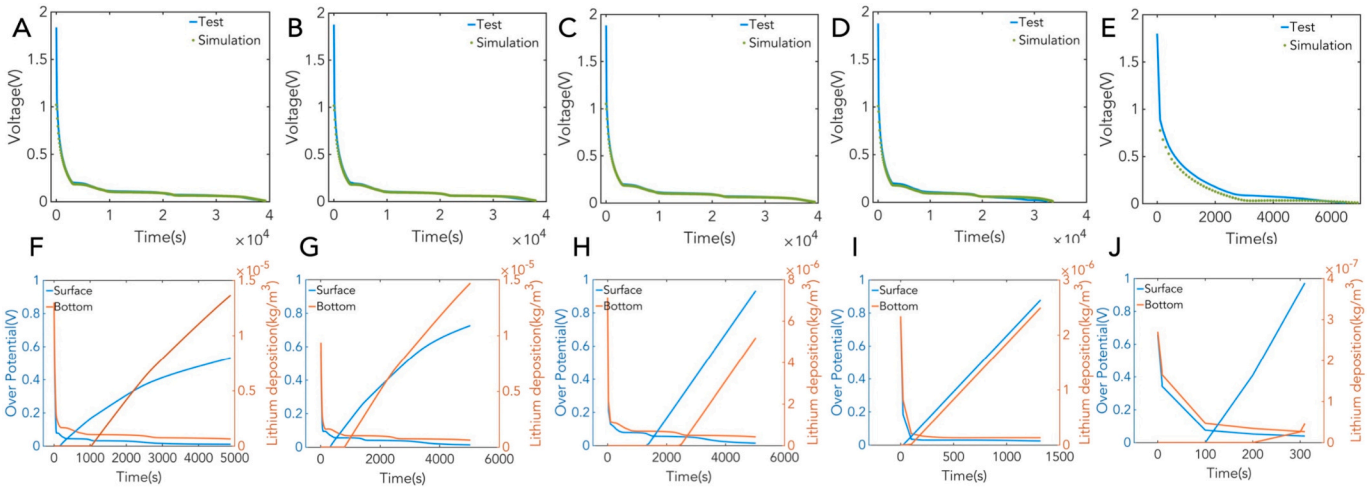

Fig. 4. The lithium deposits simulation result of graphite half cell.
The ((A), (B), (C), (D), (E)) responded to the charge rate was 0.1 C. The ((F), (G), (H), (I), (J)) responded to the charge rate was 3 C. The "surface" responded to the surface of the electrode, and the "bottom" responded to the bottom of the electrode near the collector.

kinetics ultimately prevailed in the influencing factor of lithium deposition, as the N/P value progressed. The deposition of lithium metal on the surface of the electrode and the formation of SEI will severely reduce the lithium ion diffusion coefficient of electrode (Fig. 3(H)), which makes it easier to initiate lithium deposition. Therefore, we have sufficient evidence that the direct influencing factor in lithium deposition was caused by the porosity of the electrode. The decrease in porosity does not have a greater impact on the resistivity of the battery, but it deeply affects the particle transmission in electrode, and increases the polarization in the battery, which causes more serious lithium deposition.

The pseudo-two-dimensions (P2D) simulation model of graphite half-cell was built by the COMSOL Multiphysics based on the dynamic porosity, resistivity, diffusion coefficient. Compared with the experimental data, the model we built has a higher consistency with the real battery. The lithium deposition was added in the model as the side reaction, which was described with the Butler-Volmer equation [29,40–42].

$$j_{Li} = Fk_{Li}cl^{\gamma}\left[exp\left(\frac{\alpha\eta_{Li}}{RT}\right) - exp\left(-\frac{\beta\eta_{Li}}{RT}\right)\right] \quad (\eta_{Li} < 0.05)$$

Whereas the overpotential $\eta_{Li} = \phi_s - \phi_l - E_{eq,\,Li} - \phi_{film}$, ϕ_s is the solid potential, ϕ_l is the electrolyte potential, $E_{eq,\,Li}$ is the equilibrium potential of lithium deposition that was set to 0.00 V vs. Li/Li^+. And ϕ_{film} corresponding to the film resistance due to the solid electrolyte interphase film (SEI). F is the Faraday constant, k_{Li} is the reaction rate of lithium deposition. cl is the concertation of the electrolyte. The side reaction of lithium deposition occurred when the overpotential was

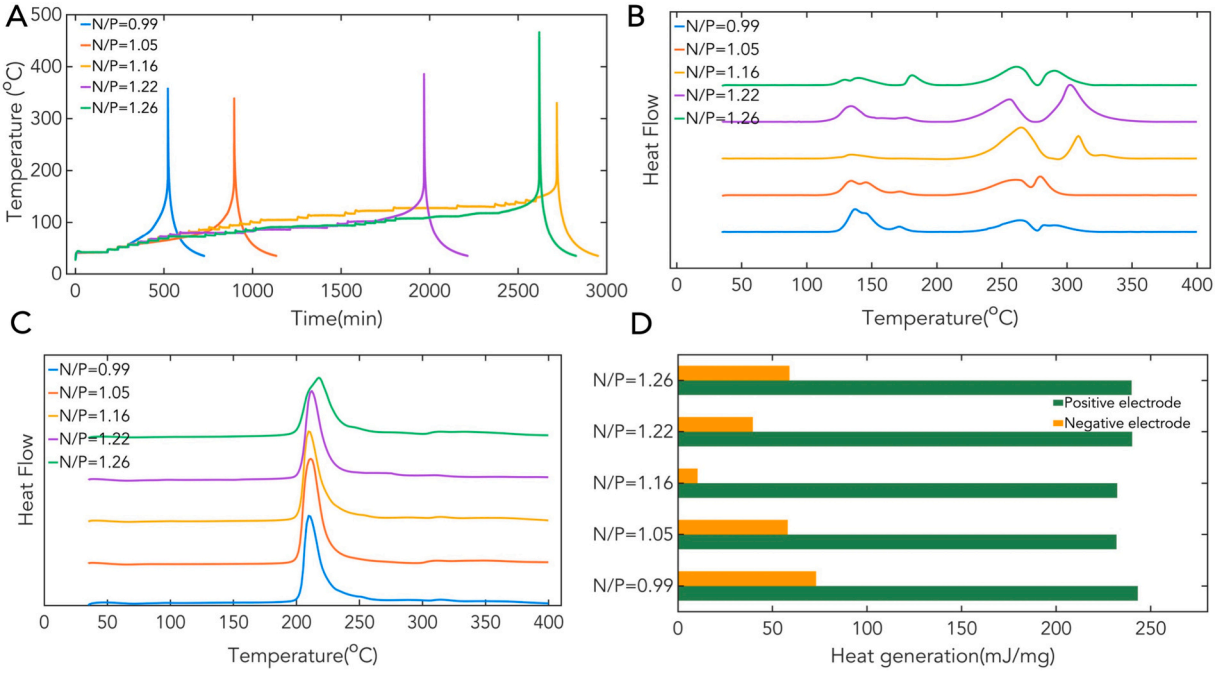

Fig. 5. Thermal safety of the different N/P batteries with lithium deposition.
(A) The ARC test result. (B) and (C) The negative, positive electrode DSC result. (D) The heat generation of the material during the test process. The electrode used in the DSC test was taken from the post-mortem test.

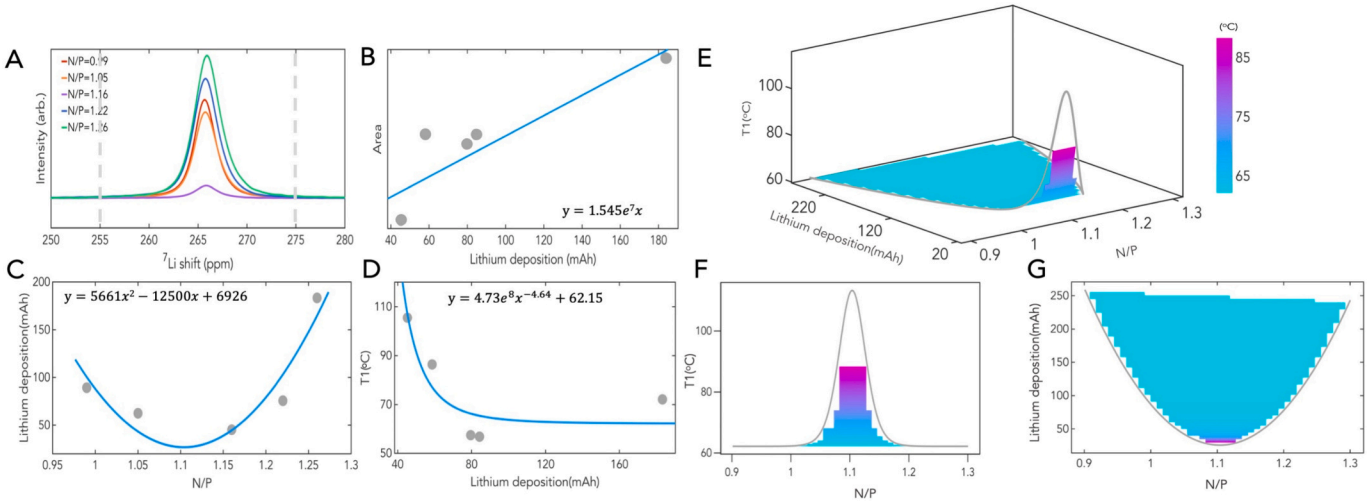

Fig. 6. The data fitting and verification of lithium deposition and safety.
(A) The NMR result of the negative electrode power. ((B), (C), (D)) The fitting result of lithium deposition. (E) The index map of the battery safety boundary. (F), (J) was selected from the side and top view of (E). The result show that the lithium deposition and the N/P value have a high linear relationship, and closely relate to the thermal runaway temperature. Meanwhile, the relationship shows the minimum value for lithium deposition at some N/P value.

lower than 0.05 V [43].

When the battery's N/P was low, the lithium deposition on the electrode surface at the end of charge will be littler than the lithium deposition at the bottom of the electrode (Fig. 4(F)), but the amount of the lithium deposition was also relatively large than other N/P value batteries, no matter surface or bottom. The amount of lithium deposition decreased as the N/P value increased is because of the constraint of cut-off voltage (Fig. 4(F)–(J)). In addition, surface deposition has gradually become the primary method of deposition, especially when the N/P value was enormous. This change in the deposition state (the deposition difference of bottom and surface) implied that there exited the possibility of uniform deposition in the lithium-ion battery.

Due to thermodynamic restriction, the battery has the unavoidable lithium deposition with the N/P smaller than 1 (even though the charging rate in the test was low). That is because the graphite electrode can't host enough lithium-ion. As the increase of N/P, the limiting factor of thermodynamic was removed, whereas the limiting factors of kinetic due to the porosity and polarization change were strengthened. The overpotential on the electrode surface was rapidly lower than 0 V, resulting in the lithium-ion not being intercalated in the negative electrode. The morphology and amount of deposited lithium were tightly related to these two factors. When the thermodynamics dominated the restriction factor, the lithium deposition site was limited by the reaction surface area, which was promoted moss-like of lithium deposition on the electrode. However, the limitation of kinetics forces lithium dendrite to occur on the electrode surface and likely uniform deposition [44–46].

3.3. Thermal safety of battery with lithium deposition

As we proposed in the front, the lithium deposition will affect the battery fast charge safety [5,47–50]. The ARC experiment of the battery was conducted after the battery was fully charged, and the batteries have been the same cycle test. There was no doubt that thermal safety will be affected by the N/P value (Fig. 5(A)). Considering the battery manufactured by the same materials, lithium deposition was inferred as the major factor affecting battery safety. Besides, the differential scanning calorimeter (DSC) test on the disassembled electrodes was performed to find the heat contribution in the process of thermal runaway. The negative electrode material has an obvious exothermic peak before 200 °C (Fig. 5(C)), while the positive electrode material has an exothermic peak between 200 and 250 °C (Fig. 5(B)). The thermal runaway of the battery occurs before 200 °C (Fig. 5(A)). Thus, it can be simply considered that the heat-generating of the negative electrode triggers the thermal runaway of the battery.

The material's heat peak was integrated to quantify the heat contribution during the whole thermal runaway process. The battery's negative electrode with the N/P value of 1.16 has the least heat release (Fig. 5(D)). However, the negative electrode of the battery with the N/P of 0.99 releases about four times more heat, and the thermal runaway of this battery occurs earlier than other batteries. Coincidentally, the battery with the N/P value of 1.26 has the same heat release. Moreover, the electrodes were confirmed to have different amounts of lithium deposition. The results fully illustrate that lithium deposition will accelerate the occurrence of battery thermal runaway. Additionally, the heat release of the lower N/P (lower than 1.16) negative electrode was higher than the larger N/P (higher than 1.16) negative electrode, and this phenomenon indicated that the dendrite lithium deposition will be more dangerous than the moss-like deposition. Meanwhile, this indicates that the dangerous caused by uniform deposition will be decreased in the same amount of lithium deposition.

3.4. Safety boundary and prediction

Although the experiments have proved the impact of lithium deposition on battery safety, they cannot quantify the impact of deposition on battery safety. Comparing the charge and discharge data of the battery before the test, a rough method was adopted to describe the amount of lithium deposition in the battery:

$$\sum_{i=1}^{N} Q_{Li,i} = Q_{charge,i} - Q_{discharge,i-1}$$

whereas the $Q_{Li,\,i}$ (mAh) represents the amount of the lithium deposition in the i cycle, the $Q_{chagre,\,i}$ represents the charge capacity of the battery in the i cycle, the $Q_{dischagre,\ i-1}$ represents the discharge capacity of the battery in the $i-1$ cycle, and the i represents the cycle number. Note that this equation can be applied to cycles at operation voltage and it does not have restriction in charge/discharge rate and material. Due to the side reactions that occur when cycling outside the operating voltage, such as the oxidative decomposition of the electrolyte, although there is a capacity performance, it is not directly related to the intercalation and deintercalation of lithium ions. Besides, The equation was based on the following assumptions:

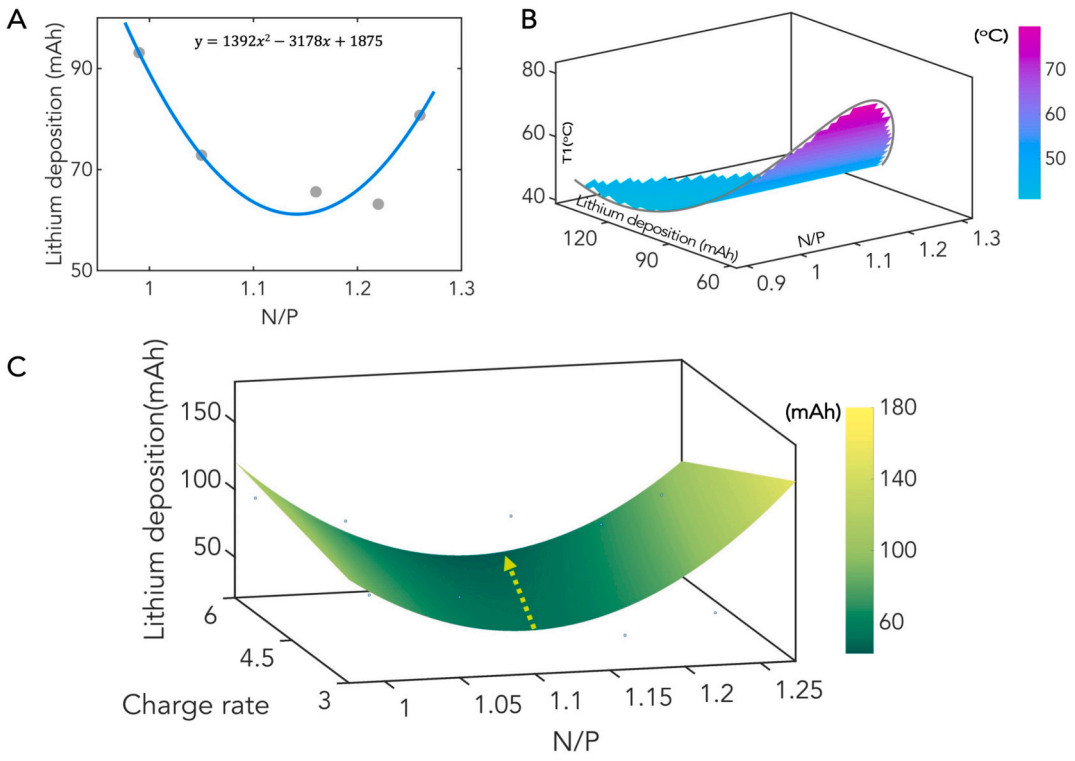

Fig. 7. The safety boundary of the battery under the fast charge rate.
(A) The fitting result of the lithium deposition and N/P. (B) The safety boundary index map under 6 C charge rate. (C) The prediction of the lithium deposition under different N/P and charge rate. Based on the relationship of lithium deposition, N/P value and thermal runaway temperature, the safety boundary was built through regression method.

1. The SEI layer in the battery has been fully formed during the activation process, which means that SEI will not be generated during the subsequent cycles.
2. The lithium deposition inside the battery and the generation of SEI are independent, which means the lithium metal formed by the deposition will not generate the SEI.
3. The deposited lithium ($Q_{Li,\ i}$) ignore the difference of dead lithium and reversible lithium. Because they are all lithium metal, no matter dead lithium and reversible lithium, affect battery safety.

The solid-state nuclear magnetic resonance (ssNMR) detection method was a more robust method to prove the formation of lithium deposition, and it can also reflect the change in the amount of deposited lithium [51–54]. The characteristic peak of metallic lithium was found at the 265 ppm shift (Fig. 6(A)) [55]. It was found that the lithium metal peak area has a strong linear relationship with the amount of lithium deposition calculated by the above method (Fig. 6(B)). It can be fully proved that the method of calculating the amount of lithium we proposed was feasible in quantifying the amount of lithium. In addition, the judgment of the amount of lithium deposition in the post-mortem process was also confirmed by the 600 MHz ssNMR.

Based on the above expression of quantitatively deposited lithium, the relation between the amount of lithium deposition and the N/P value of the battery has been constructed through a linear regression method (Fig. 6(C)). It can be found that there has a minimum value between the N/P value and the lithium deposition, and the search for the minimum was the goal of battery design and optimization. The starting of the dangerous status (T1 temperature: starting self-heat temperature) was affected by the lithium deposition. In our opinion, the battery's lithium deposition has the power function with the battery's T1 temperature. Moreover, the fitting result gave us the evidence (Fig. 6(D)). The relation of the power function indicates that the battery safety boundary was affected by the amount of lithium. In detail, the trigger of thermal runaway will no longer be affected by the amount of lithium deposition and will come to the danger statue when the amount of lithium deposition reaches the threshold.

By combining the relationship between battery lithium deposition, N/P, and T1 temperature, the battery safety boundary index map was obtained from the linear fitting (Fig. 6(E)). Indeed, the index map was built on the basis of experiments and hypotheses. If the battery is designed and used in a validated range, the operation window will be guaranteed in a safe statue, as shown in the bright part of the picture (Fig. 6(F), (G)).

3.5. *Safety design face to the fast charge battery*

The safety boundary of the battery was not static, the method we propose can be used to detect the safety state in a specific situation. However, the long charging time continuously challenges the user's patience [56]. Ultrafast charge means shorter charge time. The charging time exactly corresponds to the charging rate in index map. As stated in our above results, the lithium deposition of batteries was affected by kinetics and thermodynamics. Based on the above method, a comprehensive study on the safety of the battery at the fast charge rate was carried out.

The same battery was tested after the same charge and discharge cycle, but the constant current was set to 6 C that was because of we want to expand the index map from the factor of kinetics. The amount of lithium deposition in the battery and the N/P value still shows a highly linear relationship (Fig. 7(A)). Similarly, the safety boundary index map of the fast charge rate was obtained with the same method (Fig. 7(B)). It can be clearly seen that the T1 of the battery was sharply reduced when the battery was charged at 6 C, compared with the 3 C charge battery. This result was closely related to more amount of lithium deposits inside the battery. As the charge current increases, the amount of lithium in the battery gradually increases, and the N/P value corresponding to the

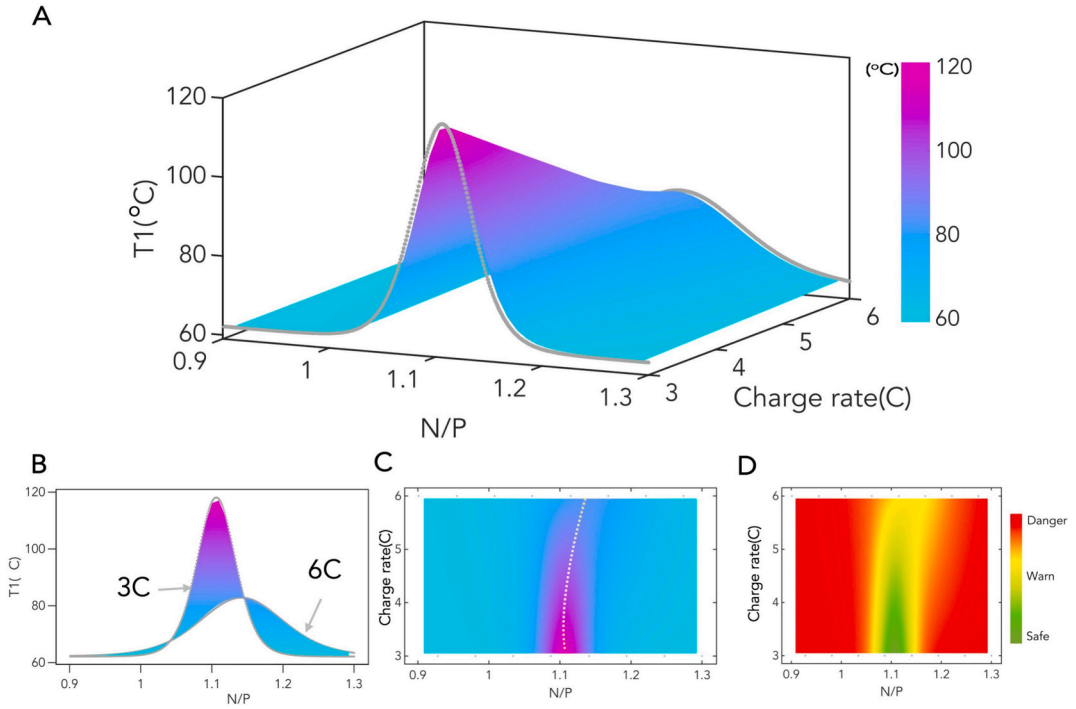

Fig. 8. The battery safety state prediction result.
The (B), (C) was the side, top view of (A). The yellow line in Fig. (C) was the best N/P value for the battery safety. The (D) present the safety range plotted according the warn temperature (70 °C). The safety boundary was extended to different charge rate to provide scientific guidance for fast charging, and the green area shown in the results can be used as the reference for battery design. (For interpretation of the references to color in this figure legend, the reader is referred to the web version of this article.)

minimum of lithium deposition also shifts to a larger value (Fig. 7(C)). The change gives the direction of N/P design and optimization when the battery needs charging at a fast charge rate.

Combining the safety boundary of the battery at different charge rate, we will get an index map of the safety state of the battery (Fig. 8). In the side view, it is evident that the T1 changes with the charge rate (Fig. 8(B)), and the best N/P value can be observed in the top view shifts to higher as the charging rate increased (as shown with the yellow line in Fig. 8(C)). The best N/P value here was the N/P value corresponding to the safest state of the battery. Besides, the most obvious feature of the chart was that the range of the best N/P became narrower as the charge rate increase (Fig. 8(C)). It means that the safety of the battery at a high charge rate will face a grave challenge, which only batteries with specific N/P value can be used safely. The 70 °C was used as the warning temperature to obtain a prediction map of the battery's safety state (Fig. 8(D)). Valuable guidance for the fast charge or battery design could be obtained from the safe area.

These results will play an essential role in the safety design of the battery. Based on the battery safety state prediction chart, the effects of economic cost, battery safety and quality all can be considered simultaneously when designing the battery. At the same time, the map also shows the safest charge rate when have been design with a constant N/P. Its dual function can ensure that the battery is in a safe state no matter the design or usage. This safety boundary provides a valuable theoretical reference for the design of fast charge batteries. In addition, according to the safety requirements of different batteries, specific architecture can be achieved. For example, the battery warning temperature can be set higher to get more safety batteries.

4. Conclusions

The disassembly of batteries with different capacity proves that there has different morphology of lithium deposition inside the batteries during the fast charge. The lithium deposition and morphology were affected by the limitation of thermodynamics and kinetics. The limitation of thermodynamics affected the moss-like deposition, but the kinetic limit was the major influence of dendritic lithium deposition. The thermal analysis confirmed that the dendrite lithium deposition in the lithium-ion battery would be more dangerous. In addition, the battery safety experiment proved that using a larger N/P value contributes to battery fast charge design. However, the quantitation of lithium deposition experiment shows that the increase of the N/P value is not absolutely essential for battery safety. In contrast, the focus of the research was the safety boundary index map which was predicted by linear regression. The safety boundary index map will provide important reference information on battery safety design and use. Significantly, the ultrafast charge and the safety of the battery will be economically realized according to the safety boundary index map. In the strict sense, the above prediction abides by the background of constant compacted density. Further exploration would be researching the safety of the lithium ion battery by quantitative lithium deposition.

CRediT authorship contribution statement

Hang Li: Conceptualization, test, Software, Methodology, Writing-Original draft preparation. **Weijie Ji:** Data curation. **Peng Zhang:** Supervision, Writing-Review & Editing. **Jinbao Zhao:** Project administration, Funding acquisition.

Declaration of competing interest

The authors declare that they have no known competing financial interests or personal relationships that could have appeared to influence the work reported in this paper.

Acknowledgements

We gratefully acknowledge the financial support of National Key

Research and Development Program of China (2017YFB0102000), National Natural Science Foundation of China (21875195), the Key Project of Science and Technology of Xiamen (3502Z20201013), the Fundamental Research Funds for the Central Universities (20720190040). We would like to thank PhD. Chaoyue Liu, Prof. Jun Cheng for their valuable guidance and suggestions. We also acknowledge Tan Kah Kee Innovation Laboratory for the engineers' help.

Appendix A. Supplementary data

Supplementary data to this article can be found online at https://doi.org/10.1016/j.est.2022.104789.

References

[1] G. Harper, R. Sommerville, E. Kendrick, L. Driscoll, P. Slater, R. Stolkin, A. Walton, P. Christensen, O. Heidrich, S. Lambert, A. Abbott, K. Ryder, L. Gaines, P. Anderson, Recycling lithium-ion batteries from electric vehicles, Nature. 575 (2019) 75–86, https://doi.org/10.1038/s41586-019-1682-5.

[2] P.R. Shearing, L.R. Johnson, Toward practical demonstration of high-energy-density batteries, Joule. 4 (2020) 1359–1361, https://doi.org/10.1016/j.joule.2020.06.019.

[3] S. Wang, Q. Liu, C. Zhao, F. Lv, X. Qin, H. Du, F. Kang, B. Li, Advances in understanding materials for rechargeable lithium batteries by atomic force microscopy, Energy Environ. Mater. 1 (2018) 28–40, https://doi.org/10.1002/eem2.12002.

[4] G. Xu, L. Huang, C. Lu, X. Zhou, G. Cui, Revealing the multilevel thermal safety of lithium batteries, Energy Storage Mater. 31 (2020) 72–86, https://doi.org/10.1016/j.ensm.2020.06.004.

[5] X. Feng, M. Ouyang, X. Liu, L. Lu, Y. Xia, X. He, Thermal runaway mechanism of lithium ion battery for electric vehicles: a review, Energy Storage Mater. 10 (2018) 246–267, https://doi.org/10.1016/j.ensm.2017.05.013.

[6] G.-L. Zhu, C.-Z. Zhao, H. Yuan, B.-C. Zhao, L.-P. Hou, X.-B. Cheng, H.-X. Nan, Y. Lu, J. Zhang, J.-Q. Huang, Q.-B. Liu, C.-X. He, Q. Zhang, Interfacial redox behaviors of sulfide electrolytes in fast-charging all-solid-state lithium metal batteries, Energy Storage Mater. 31 (2020) 267–273, https://doi.org/10.1016/j.ensm.2020.05.017.

[7] S.S. Zhang, The puzzles in fast charging of Li-ion batteries, Energy Environ. Mater. (2021) eem2.12330, https://doi.org/10.1002/eem2.12330.

[8] X.-G. Yang, T. Liu, Y. Gao, S. Ge, Y. Leng, D. Wang, C.-Y. Wang, Asymmetric temperature modulation for extreme fast charging of Lithium-ion batteries, Joule. 3 (2019) 3002–3019, https://doi.org/10.1016/j.joule.2019.09.021.

[9] X.-G. Yang, T. Liu, S. Ge, E. Rountree, C.-Y. Wang, Challenges and key requirements of batteries for electric vertical takeoff and landing aircraft, Joule. 5 (2021) 1644–1659, https://doi.org/10.1016/j.joule.2021.05.001.

[10] T.R. Tanim, E.J. Dufek, M. Evans, C. Dickerson, A.N. Jansen, B.J. Polzin, A. R. Dunlop, S.E. Trask, R. Jackman, I. Bloom, Z. Yang, E. Lee, Extreme fast charge challenges for lithium-ion battery: variability and positive electrode issues, journal of the electrochemical, Society (2019) 14.

[11] Y. Liu, Y. Cui, Lithium metal anodes: a recipe for protection, Joule 1 (2017) 649–650, https://doi.org/10.1016/j.joule.2017.12.001.

[12] T. Gao, Y. Han, D. Fraggedakis, S. Das, T. Zhou, C.-N. Yeh, S. Xu, W.C. Chueh, J. Li, M.Z. Bazant, Interplay of lithium intercalation and plating on a single graphite particle, Joule. 5 (2021) 393–414, https://doi.org/10.1016/j.joule.2020.12.020.

[13] Z. Liu, Y. Jiang, Q. Hu, S. Guo, L. Yu, Q. Li, Q. Liu, X. Hu, Safer lithium-ion batteries from the separator aspect: development and future perspectives, Energy Environ. Mater. 4 (2021) 336–362, https://doi.org/10.1002/eem2.12129.

[14] J. Pu, J. Li, K. Zhang, T. Zhang, C. Li, H. Ma, J. Zhu, P.V. Braun, J. Lu, H. Zhang, Conductivity and lithiophilicity gradients guide lithium deposition to mitigate short circuits, Nat. Commun. 10 (2019) 1896, https://doi.org/10.1038/s41467-019-09932-1.

[15] X. Chen, B. Zhao, C. Yan, Q. Zhang, Review on Li deposition in working batteries: from nucleation to early growth, Adv. Mater. 33 (2021) 2004128, https://doi.org/10.1002/adma.202004128.

[16] X. Guan, A. Wang, S. Liu, G. Li, F. Liang, Y.-W. Yang, X. Liu, J. Luo, Controlling nucleation in lithium metal anodes, Small 14 (2018) 1801423, https://doi.org/10.1002/smll.201801423.

[17] T. Waldmann, Li plating as unwanted side reaction in commercial Li-ion cells – a review, J. Power Sources 18 (2018).

[18] L. Li, S. Li, Y. Lu, Suppression of dendritic lithium growth in lithium metal-based batteries, Chem. Commun. 54 (2018) 6648–6661, https://doi.org/10.1039/C8CC02280A.

[19] P.P. Paul, E.J. McShane, A.M. Colclasure, N. Balsara, D.E. Brown, C. Cao, B. Chen, P.R. Chinnam, Y. Cui, E.J. Dufek, D.P. Finegan, S. Gillard, W. Huang, Z.M. Konz, R. Kostecki, F. Liu, S. Lubner, R. Prasher, M.B. Preefer, J. Qian, M.F. Rodrigues, M. Schnabel, S. Son, V. Srinivasan, H. Steinrück, T.R. Tanim, M.F. Toney, W. Tong, F. Usseglio-Viretta, J. Wan, M. Yusuf, B.D. McCloskey, J. Nelson Weker, A review of existing and emerging methods for lithium detection and characterization in Li-ion and Li-metal batteries, Adv. Energy Mater. 11 (2021), 2100372, https://doi.org/10.1002/aenm.202100372.

[20] X. Lin, K. Khosravinia, X. Hu, J. Li, W. Lu, Lithium plating mechanism, detection, and mitigation in lithium-ion batteries, Prog. Energy Combust. Sci. 87 (2021), 100953, https://doi.org/10.1016/j.pecs.2021.100953.

[21] P. Arora, M. Doyle, R.E. White, Mathematical modeling of the lithium deposition overcharge reaction in lithium-ion batteries using carbon-based negative electrodes, J. Electrochem. Soc. 146 (1999) 3543–3553, https://doi.org/10.1149/1.1392512.

[22] M. Tang, P. Albertus, J. Newman, Two-dimensional modeling of lithium deposition during cell charging, J. Electrochem. Soc.. (n.d.) 11.

[23] W. Chen, Y. Hu, W. Lv, T. Lei, X. Wang, Z. Li, M. Zhang, J. Huang, X. Du, Y. Yan, W. He, C. Liu, M. Liao, W. Zhang, J. Xiong, C. Yan, Lithiophilic montmorillonite serves as lithium ion reservoir to facilitate uniform lithium deposition, Nat. Commun. 10 (2019) 4973, https://doi.org/10.1038/s41467-019-12952-6.

[24] R. Pathak, K. Chen, A. Gurung, K.M. Reza, B. Bahrami, J. Pokharel, A. Baniya, W. He, F. Wu, Y. Zhou, K. Xu, Q. (Quinn) Qiao, Fluorinated hybrid solid-electrolyte-interphase for dendrite-free lithium deposition, Nat. Commun. 11 (2020) 93, https://doi.org/10.1038/s41467-019-13774-2.

[25] Z. Li, J. Huang, B. Yann Liaw, V. Metzler, J. Zhang, A review of lithium deposition in lithium-ion and lithium metal secondary batteries, J. Power Sources 254 (2014) 168–182, https://doi.org/10.1016/j.jpowsour.2013.12.099.

[26] M. Ouyang, Z. Chu, L. Lu, J. Li, X. Han, X. Feng, G. Liu, Low temperature aging mechanism identification and lithium deposition in a large format lithium iron phosphate battery for different charge profiles, J. Power Sources 286 (2015) 309–320, https://doi.org/10.1016/j.jpowsour.2015.03.178.

[27] J. Sieg, J. Bandlow, T. Mitsch, D. Dragicevic, T. Materna, B. Spier, H. Witzenhausen, M. Ecker, D.U. Sauer, Fast charging of an electric vehicle lithium-ion battery at the limit of the lithium deposition process, J. Power Sources 427 (2019) 260–270, https://doi.org/10.1016/j.jpowsour.2019.04.047.

[28] K. Märker, C. Xu, C.P. Grey, Operando NMR of NMC811/graphite lithium-ion batteries: structure, dynamics, and lithium metal deposition, J. Am. Chem. Soc. 10 (2020).

[29] D. Ren, K. Smith, D. Guo, X. Han, X. Feng, L. Lu, M. Ouyang, J. Li, Investigation of lithium plating-stripping process in Li-ion batteries at low temperature using an electrochemical model, J. Electrochem. Soc. 165 (2018) A2167–A2178, https://doi.org/10.1149/2.0661810jes.

[30] W. Zhang, D.-H. Seo, T. Chen, L. Wu, M. Topsakal, Y. Zhu, D. Lu, G. Ceder, F. Wang, Kinetic pathways of ionic transport in fast-charging lithium titanate 6 (2020).

[31] Q. Liu, C. Du, B. Shen, P. Zuo, X. Cheng, Y. Ma, G. Yin, Y. Gao, Understanding undesirable anode lithium plating issues in lithium-ion batteries, RSC Adv. 6 (2016) 88683–88700, https://doi.org/10.1039/C6RA19482F.

[32] M.C. Smart, B.V. Ratnakumar, Effects of electrolyte composition on lithium plating in lithium-ion cells, J. Electrochem. Soc. 158 (2011) A379–A389, https://doi.org/10.1149/1.3544439.

[33] J. Cannarella, C.B. Arnold, The effects of defects on localized plating in lithium-ion batteries, J. Electrochem. Soc. 162 (2015) A1365–A1373, https://doi.org/10.1149/2.1051507jes.

[34] K.G. Gallagher, S.E. Trask, C. Bauer, T. Woehrle, S.F. Lux, M. Tschech, P. Lamp, B. J. Polzin, S. Ha, B. Long, Q. Wu, W. Lu, D.W. Dees, A.N. Jansen, Optimizing areal capacities through understanding the limitations of lithium-ion electrodes, J. Electrochem. Soc. 163 (2016) A138–A149, https://doi.org/10.1149/2.0321602jes.

[35] L. Ren, A. Wang, X. Zhang, G. Li, X. Liu, J. Luo, Eliminating dendrites through dynamically engineering the forces applied during Li deposition for stable lithium metal anodes, Adv. Energy Mater. 10 (2020) 1902932, https://doi.org/10.1002/aenm.201902932.

[36] X.-B. Cheng, T.-Z. Hou, R. Zhang, H.-J. Peng, C.-Z. Zhao, J.-Q. Huang, Q. Zhang, Dendrite-free lithium deposition induced by uniformly distributed lithium ions for efficient lithium metal batteries, Adv. Mater. 28 (2016) 2888–2895, https://doi.org/10.1002/adma.201506124.

[37] V. Ramadesigan, P.W.C. Northrop, S. De, S. Santhanagopalan, R.D. Braatz, V. R. Subramanian, Modeling and simulation of lithium-ion batteries from a systems engineering perspective, J. Electrochem. Soc. 159 (2012) R31–R45, https://doi.org/10.1149/2.018203jes.

[38] S. Li, S. Fang, H. Dou, X. Zhang, RbF as a dendrite-inhibiting additive in lithium metal batteries, ACS Appl. Mater. Interfaces 11 (2019) 20804–20811, https://doi.org/10.1021/acsami.9b03940.

[39] W. Mei, L. Jiang, C. Liang, J. Sun, Q. Wang, Understanding of Li-plating on graphite electrode: detection, quantification and mechanism revelation, Energy Storage Mater. 41 (2021) 209–221, https://doi.org/10.1016/j.ensm.2021.06.013.

[40] S. Hein, T. Danner, A. Latz, An electrochemical model of Lithium plating and stripping in lithium ion batteries, ACS Appl. Energy Mater. 3 (2020) 8519–8531, https://doi.org/10.1021/acsaem.0c01155.

[41] J. Keil, A. Jossen, Electrochemical modeling of linear and nonlinear aging of lithium-ion cells, J. Electrochem. Soc. 167 (2020), 110535, https://doi.org/10.1149/1945-7111/aba44f.

[42] M. Song, S.-Y. Choe, Fast and safe charging method suppressing side reaction and lithium deposition reaction in lithium ion battery, J. Power Sources 436 (2019) 226835, https://doi.org/10.1016/j.jpowsour.2019.226835.

[43] B. Wang, L.L. Fevre, A. Brookfield, E. McInnes, R.A.W. Dryfe, Resolution of Li deposition vs intercalation of graphite anodes in lithium ion batteries - an in situ electron paramagnetic resonance study, Angew. Chem. Int. Ed. (n.d.) 9.

[44] Y. Liu, S. Xiong, J. Wang, X. Jiao, S. Li, C. Zhang, Z. Song, J. Song, Dendrite-free lithium metal anode enabled by separator engineering via uniform loading of lithiophilic nucleation sites, Energy Storage Mater. 19 (2019) 24–30, https://doi.org/10.1016/j.ensm.2018.10.015.

[45] B. Liu, Y. Zhang, G. Pan, C. Ai, S. Deng, S. Liu, Q. Liu, X. Wang, X. Xia, J. Tu, Ordered lithiophilic sites to regulate Li plating/stripping behavior for superior lithium metal anodes, J. Mater. Chem. A 7 (2019) 21794–21801, https://doi.org/10.1039/C9TA09502K.

[46] G. Li, Regulating mass transport behavior for high-performance lithium metal batteries and fast-charging lithium-ion batteries, Adv. Energy Mater. 11 (2021) 2002891, https://doi.org/10.1002/aenm.202002891.
[47] T. Waldmann, M. Wohlfahrt-Mehrens, Effects of rest time after Li plating on safety behavior—ARC tests with commercial high-energy 18650 Li-ion cells, Electrochim. Acta 230 (2017) 454–460, https://doi.org/10.1016/j.electacta.2017.02.036.
[48] Y. Jiang, Z. Wang, C. Xu, W. Li, Y. Li, S. Huang, Z. Chen, B. Zhao, X. Sun, D. P. Wilkinson, J. Zhang, Atomic layer deposition for improved lithiophilicity and solid electrolyte interface stability during lithium plating, Energy Storage Mater. 28 (2020) 17–26, https://doi.org/10.1016/j.ensm.2020.01.019.
[49] Q. Wang, B. Mao, S.I. Stoliarov, J. Sun, A review of lithium ion battery failure mechanisms and fire prevention strategies, Prog. Energy Combust. Sci. 73 (2019) 95–131, https://doi.org/10.1016/j.pecs.2019.03.002.
[50] S. Abada, G. Marlair, A. Lecocq, M. Petit, V. Sauvant-Moynot, F. Huet, Safety focused modeling of lithium-ion batteries: a review, J. Power Sources 306 (2016) 178–192, https://doi.org/10.1016/j.jpowsour.2015.11.100.
[51] H.J. Chang, N.M. Trease, A.J. Ilott, D. Zeng, L.-S. Du, A. Jerschow, C.P. Grey, Investigating Li microstructure formation on Li anodes for lithium batteries by in situ ^{6}Li/ ^{7}Li NMR and SEM, J. Phys. Chem. C 119 (2015) 16443–16451, https://doi.org/10.1021/acs.jpcc.5b03396.
[52] K. Märker, C. Xu, C.P. Grey, Operando NMR of NMC811/graphite lithium-ion batteries: structure, dynamics, and lithium metal deposition, J. Am. Chem. Soc. 142 (2020) 17447–17456, https://doi.org/10.1021/jacs.0c06727.
[53] L.E. Marbella, S. Zekoll, J. Kasemchainan, S.P. Emge, P.G. Bruce, C.P. Grey, ^{7}Li NMR chemical shift imaging to detect microstructural growth of lithium in all-solid-state batteries, Chem. Mater. 31 (2019) 2762–2769, https://doi.org/10.1021/acs.chemmater.8b04875.
[54] A.B. Gunnarsdóttir, C.V. Amanchukwu, S. Menkin, C.P. Grey, Noninvasive *in situ* NMR study of “dead lithium” formation and lithium corrosion in full-cell lithium metal batteries, J. Am. Chem. Soc. 142 (2020) 20814–20827, https://doi.org/10.1021/jacs.0c10258.
[55] J. Arai, R. Nakahigashi, Study of Li metal deposition in Lithium ion battery during low-temperature cycle using in situ solid-state ^{7}Li nuclear magnetic resonance, J. Electrochem. Soc. 164 (2017) A3403–A3409, https://doi.org/10.1149/2.1921713jes.
[56] S. Ahmed, I. Bloom, A.N. Jansen, T. Tanim, E.J. Dufek, A. Pesaran, A. Burnham, R. B. Carlson, F. Dias, K. Hardy, M. Keyser, C. Kreuzer, A. Markel, A. Meintz, C. Michelbacher, M. Mohanpurkar, P.A. Nelson, D.C. Robertson, D. Scoffield, M. Shirk, T. Stephens, R. Vijayagopal, J. Zhang, Enabling fast charging – a battery technology gap assessment, J. Power Sources 367 (2017) 250–262, https://doi.org/10.1016/j.jpowsour.2017.06.055.